A primer on inference and prediction with epidemic renewal models using sequential Monte Carlo methods

Nicholas Steyn

28 October 2024

Contents

Abstract

Renewal models are widely employed in statistical epidemiology as semi-mechanistic models of disease transmission. While primarily used for estimating the instantaneous reproduction number, they can also be used for forecasting, estimating elimination probabilities, modelling the effect of interventions, and more. We demonstrate how simple sequential Monte Carlo methods can be used to perform inference on these models. Our goal is to acquaint readers with a working knowledge of statistical inference to these methods and models, and to provide a practical guide to their implementation. We focus on the flexibility of these methods and their ability to handle multiple biases simultaneously and leverage this flexibility to unify existing methods for reproduction number estimation and epidemic forecasting. A companion website SMC and epidemic renewal models contains additional worked examples and self-contained code to reproduce the examples presented here.

1 Introduction

Modern epidemiology relies on statistical models and methods to track and forecast the spread of infectious diseases, inform public health policymaking, communicate with the wider public, and estimate disease burden [1]. A commonly used model for these purposes is the semi-mechanistic renewal model, which relates past incidence to current incidence through a simple renewal process [2]. While this model is typically used for estimating the instantaneous reproduction number R_t [3, 4, 5], it can also be used for forecasting [6], estimating elimination probabilities [7], and modelling the effect of public health interventions [8], among other applications. Modifications to renewal models, accounting for various biases and limitations in epidemiological data, are common in the literature [9]. These modifications often necessitate bespoke methods for fitting the model to data, which can be difficult to implement and increase in complexity as more modifications are required. We propose the use of sequential Monte Carlo (SMC) methods [10] as a flexible and general-purpose solution to fitting renewal models to data, which can handle multiple biases simultaneously and provide a unified framework for reproduction number estimation and epidemic forecasting.

Reviews of reproduction number estimation in particular raise many practical considerations that can negatively impact the accuracy of estimates. Gostic et al. [11] highlight generation interval misspecification, reporting delays, right-truncation, incomplete observation, and smoothing windows. Nash, Nouvellet, and Cori [9] identify 54 papers that make modifications to EpiEstim (just one of many methods for estimating the reproduction number) to account for such biases. They identified delayed/missing case reporting, weekly reporting noise, alternative smoothing methods, accounting for imported cases, and temporal aggregation of reported data (among others) as common modifications. These adjustments are just as necessary for forecasting and other forms of inference as they are for R_t estimation.

SMC methods, despite being well suited to fitting epidemiological models, having a relatively straightforward and intuitive implementation, and calls for their further use [12], are not widely used in statistical epidemiology. The epidemiological studies that do leverage SMC methods typically fit mechanistic SIR-type models [13, 14, 15, 15, 16, 17, 18, 19], although examples of their use in agent-based models [20] and renewal models [21, 22] also exist.

We are aware of two reviews of SMC methods in epidemiology [23, 24]. In particular, Temfack and Wyse [23] provide an excellent explanation of some concepts we touch on, using similar notation, and we encourage the interested reader to consider this paper also. Both of these reviews focus on using SMC to fit more traditional mechanistic models, rather than the renewal model, however. To assist with the joint interpretation of these papers, a full discussion of similarities and differences are provided online.

Our goal is to acquaint the reader with both the renewal model and SMC methods. We provide simple implementations of SMC-type algorithms (a bootstrap filter with fixed-lag resampling, and a particle marginal Metropolis-Hastings (PMMH) algorithm) for fitting renewal models to data, and demonstrate their use in a handful of scenarios, leveraging data from the COVID-19 pandemic in Aotearoa New Zealand. Guidance on model evaluation and comparison is also provided. We emphasise that our goal is not to provide a model for every possible scenario, but instead to equip the reader with the tools to easily construct and fit their own models. While

this paper contains all technical information necessary to construct these models, users may find it easier to start with the example code, referring to this paper as required. All code required to reproduce these examples is available online in *SMC and epidemic renewal models*.

2 Hidden-state models and the renewal model

SMC methods are a class of algorithms for fitting general hidden-state models to data [10]. A hidden-state model consists of time and/or space-indexed hidden states X_t, observed data y_t, and parameter(s) θ. The model structure is defined by a probabilistic sequential state-space model $P(X_t|X_{1:t-1}, \theta)$, which dictates how hidden states vary from one time step to the next, and an observation model $P(y_t|X_{1:t-1}, y_{1:t-1}, \theta)$, which relates observed data to the hidden states. In theory, any model that can be written in this form can be solved using SMC methods. This is a particularly convenient structure in epidemiology, where the underlying epidemic process (such as infection incidence and the reproduction number) forms the hidden states, from which we observe some data (such as reported cases).

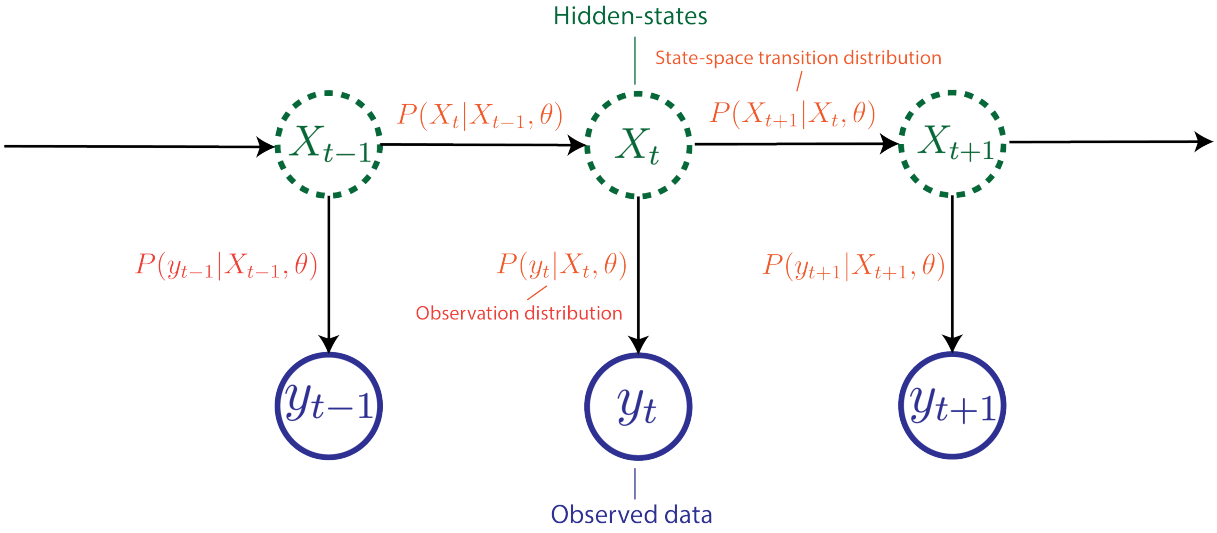

Figure 1: A diagram of a simple hidden-state model. In this example, hidden states X_t depend only on the previous hidden state X_{t-1}, and observed data y_t depend only on the hidden state at time t. This particular example is known as a Hidden Markov Model, although SMC methods can also solve more complex models.

Many popular epidemic models can be written in this form. EpiFilter, which can be used to estimate the instantaneous reproduction number R_t [5] or model the elimination probability of an epidemic [7], is explicitly described as a hidden state model where hidden-state R_t is assumed to follow a Gaussian random walk (the hidden-state model) and observed cases C_t are assumed to follow the Poisson renewal model (the observation model). Less obvious is the model of Fraser et al. [25], which uses the same observation model as EpiFilter, but assumes R_t is piecewise constant on intervals of 10 days. Further examples include the random walk implementation of EpiNow2 [4], and a model for temporally aggregated and underreported data by Ogi-Gittins et al. [26]. These models were solved using bespoke methods, such as a grid-based approximation to the Bayesian filtering and smoothing equations in EpiFilter, maximum likelihood estimation in Fraser et al. [25], or a bespoke MCMC algorithm in EpiNow2 [4].

While SMC methods can be used to fit a wide range of models, we focus on the epidemic renewal

model in this primer. Denoting reported cases at time t by C_t, the reproduction number by R_t, and the serial interval (the probability that a secondary infection was reported u days after the primary infection) by ω_u, the renewal model describes the expected value of reported cases at time t as:

$$E[C_t] = R_t \sum_{u=1}^{u_{max}} C_{t-u}\omega_u \tag{1}$$

If C_t is assumed to be Poisson distributed with mean $E[C_t]$, then we have the popular Poisson renewal model, although other distributions can be (and are) used [27]. We also note that while the renewal model is often implemented on reported cases, we can replace the serial interval ω_u with a generation time distribution g_u, and apply the model to unobserved incidence instead. This is particularly useful in the presence of reporting noise (sections 5.2 and 5.3).

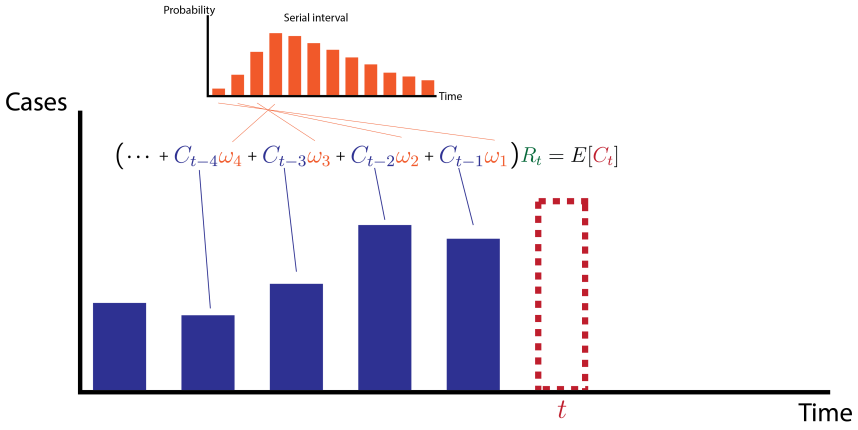

Figure 2: A diagram of the renewal model showing how past reported cases are convolved with a serial interval distribution to estimate the expected number of reported cases at time t, conditional on R_t.

3 Sequential Monte-Carlo methods

We introduce two SMC-type algorithms for fitting the renewal model to data. The first is a bootstrap filter, which takes observed data $y_{1:T}$ and parameter(s) θ as inputs, and returns the smoothing posterior distribution at each step $P(X_t|y_{1:T}, \theta)$. The "smoothing" here refers to the fact that X_t depends on both past $y_{1:t}$ and future data $y_{t+1:T}$ [5]. If our goal is to estimate the hidden states conditional on pre-determined parameters θ (such as R_t given a fixed level of smoothing), then we are finished.

The second algorithm is PMMH, which takes observed data $y_{1:T}$ as inputs and returns the posterior distribution of the parameter(s) θ, denoted $P(\theta|y_{1:T})$. If our goal is to learn about θ itself, then we are finished. If our goal is to forecast or perform inference on hidden states X_t without conditioning on θ, then we can use this posterior distribution to find the marginal smoothing posterior distribution $P(X_t|y_{1:T})$ (section 4.1).

These methods are general-purpose and can be applied to any hidden-state model defined by a state-space transition model $P(X_t|X_{1:t-1}, \theta)$ and a probabilistic observation model $P(y_t|X_{1:t}, y_{1:t-1}, \theta)$. To guide intuition, it can be helpful to consider X_t as the reproduction number R_t and y_t as

reported cases C_t.

3.1 The bootstrap filter

The goal of the bootstrap filter [28] is to find the smoothing posterior distribution $P(X_t|y_{1:T}, \theta)$, such as the posterior distribution of R_t given observed cases $C_{1:T}$ and parameter(s) θ, at each time step t. This is achieved by constructing a set of "particles" $\{x_t^{(i)}\}_{i=1}^N$ representing draws from this target distribution which can then be used to calculate quantities like the posterior mean and credible intervals.

We start with an initial set of particles $\{x_0^{(i)}\}$ for $i = 1, \ldots, N$ sampled from an initial-state distribution $P(X_0)$. These particles are projected forward by sampling from the state-space transition model $\tilde{x_t}^{(i)} \sim P(X_t|x_{1:t-1}, \theta)$, representing equally likely one-step-ahead forecasts of the hidden states before any data are observed. These projections are weighted by the observation model $w_t^{(i)} = P(y_t|\tilde{x_t}^{(i)}, y_{1:t-1}, \theta)$, describing how likely each projected particle is once the data at time step t are observed. The particles are then resampled with replacement according to these weights, resulting in a new set of particles $\{x_t^{(i)}\}_{i=1}^N$ that represent samples from the posterior distribution at time step t. This process is described in figure 3. Repeating this process for $t = 1, \ldots, T$ completes the algorithm (algorithm 1).

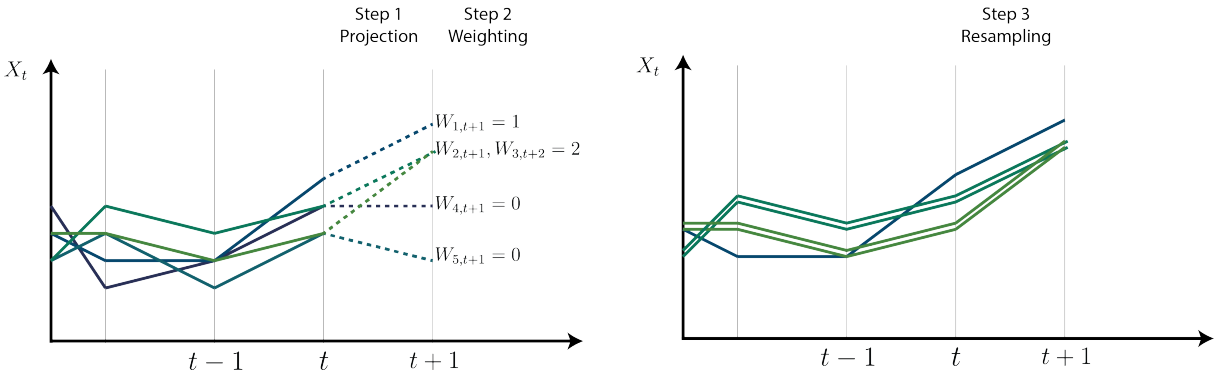

Figure 3: A single step of the bootstrap filter with resampling. Particles are projected forward by sampling according to the state-space transition model, weighted by the observation model, and resampled to form a new set of particles.

If only the particles at time step t are resampled, then the filtering distribution $P(X_t|y_{1:t}, \theta)$ is returned. If all particle histories are also resampled at each time step, then the smoothing distribution $P(X_t|y_{1:T}, \theta)$ is returned. When T is large, resampling all particle histories at each time step can lead to particle degeneracy, where very few unique particles remain at small values of t (observed in figure 3 by the decreasing number of unique particle trajectories after resampling), leading to poor approximations of the smoothing distribution.

To mitigate particle degeneracy, we introduce fixed-lag resampling, only resampling the past L time steps. This results in an approximation to the smoothing distribution $P(X_t|y_{1:t+L}, \theta)$, which, if L is chosen such that $y_{t+L:T}$ is conditionally independent of $y_{1:t}$ given X_t, is equivalent to the true smoothing distribution. Intuitively, this is assuming that observed data L time steps into the future are independent of observed data today, given knowledge of the underlying hidden states today, an assumption we can commonly make in infectious-disease epidemiology. The fixed-lag resampling also ensures that the particles from the final L time steps $\{x_{T-L:T}^{(i)}\}$ are

samples from the joint distribution $P(X_{T-L,T}|y_{1:T}, \theta)$ which is useful when estimating quantities such as the timing of epidemic peaks.

Algorithm 1 The fixed-lag bootstrap filter. Statements indexed by i should be taken to mean for i in $\{1, 2, \ldots, N\}$. At time step t, $\tilde{X}_{i,t-L:t}$ is taken to mean the aggregation of particle history $X_{i,t-L:t-1}$ and newly projected particles $\tilde{X}_{i,t}$.

1: **Input:** Number of particles N, fixed lag L, parameter(s) θ, data $y_{1:T}$, state-space transition model $P(X_t|X_{1:t-1}, \theta)$, observation model $P(y_t|X_{1:t}, y_{1:t-1}, \theta)$, and initial state-space distribution $P(X_0)$
2: **Initialise:** $X_{i,0} \sim P(X_0)$
3: **for** $t = 1$ to T **do**
4: $\quad \tilde{x}_{i,t} \sim P(X_t|x_{i,1:t-1}, \theta)$ ▷ Sample from the state-space transition model
5: $\quad W_{i,t} \leftarrow P(y_t|\tilde{x}_{i,t-L:t}, y_{1:t-1}, \theta)$ ▷ Calculate the observation weights
6: $\quad x_{i,t-L:t} \sim \text{Mulitnomial}\left(\{\tilde{x}_{\cdot,t-L:t}\}, \{W_{\cdot,t}\}\right)$ ▷ Resample the particles
7: **end for**
8: **Return:** Particle values $x_{i,t}$ and observation weights $W_{i,t}$ for $i = 1, \ldots, N$ and $t = 1, \ldots T$.

Practical considerations

In addition to the choice of fixed lag L, there are a number of practical aspects to consider.

The number of particles N should be chosen to balance computational efficiency and accuracy. The appropriate number depends on the complexity of the model, how well the model fits the data, and the purpose of the bootstrap filter. In practice, we find that $N = 100,000$ is sufficient for all models we consider when the aim is hidden-state inference. This can be decreased (typically to $N = 1000$) when the algorithm is used for likelihood estimation (section 3.2) or when the algorithm is used to find the marginal smoothing posterior distribution (section 4.1). The choice of N for a specific model can be guided by comparing hidden-state estimates across different runs: if the estimates are stable, then N is likely sufficiently large.

In algorithm 1, for simplicity, we use the state-space transition distribution as the proposal distribution (algorithm 1, line 4). This is known to be suboptimal, particularly because it does not use information about the observed data y_t when proposing new particles. More complex proposal distributions can be employed and the weights (algorithm 1, line 5) adjusted to account for the fact that the proposal distribution is not the true state-space transition distribution. One such example is the auxiliary particle filter [29], although we find this unnecessary for the models fit in this primer.

Model outputs are usually robust to the reasonable choice of initial state distribution $P(X_0)$. In the absence of clear prior information, this should be chosen such that any plausible value of X_0 is possible.

A large proportion of SMC-literature focusses on hidden Markov Models. In this primer we apply SMC methods to non-Markovian models (i.e. those where X_t depends on $X_{1:t-1}$ rather than just X_{t-1}). To ensure past particle trajectories are consistent, fixed-lag resampling must be used when fitting non-Markovian models. In these cases, L should be chosen such that X_t does not depend on hidden-state values prior to $t - L$.

3.2 Particle marginal Metropolis-Hastings

The goal of the PMMH algorithm [30] is to find the posterior distribution of parameter(s) θ, given observed data $y_{1:T}$. We do this by employing a simple Metropolis-Hastings algorithm [31], while using SMC (algorithm 1) to estimate the likelihood of the proposed parameters.

The log-likelihood estimator is given by the sum of the logarithm of the mean particle weights $\bar{w}_t$ from the bootstrap filter (algorithm 1) at each time step:

$$\hat{\ell}(\theta|y_{1:T}) = \frac{1}{T}\sum_{t=1}^{T} \log \bar{w}_t \tag{2}$$

This follows immediately from the predictive decomposition of the likelihood:

$$\ell(\theta|y_{1:T}) = \log P(y_{1:T}|\theta) = \log \prod_{t=1}^{T} P(y_t|y_{1:t-1}, \theta) \tag{3}$$

where a Monte-Carlo estimator of the one-step-ahead predictive likelihood is given by $\bar{w}_t$:

$$\begin{aligned} P(y_t|y_{1:t-1}, \theta) &= E_{X_{1:t}|y_{1:t-1}}\left[P(y_t|X_{1:t}, y_{1:t-1}, \theta)\right] \\ &\approx \frac{1}{N}\sum_{i=1}^{N} P(y_t|\tilde{X}_{i,t}, y_{1:t-1}, \theta) \\ &= \bar{w}_t \end{aligned} \tag{4}$$

Parameter inference thus involves using $\hat{\ell}(\theta|y_{1:T})$ in the acceptance probability of an otherwise standard Metropolis-Hastings algorithm (algorithm 2).

Algorithm 2 Particle marginal Metropolis Hastings (PMMH). The bootstrap filter $\mathcal{M}$ written here accepts proposed parameters θ' and returns a matrix of weights. The data $y_{1:T}$ and other bootstrap filter options are assumed to be included in $\mathcal{M}$.

Input: Number of parameter samples N_θ, bootstrap filter $\mathcal{M}$, parameter prior distribution $P(\theta)$, parameter proposal distribution $P(\theta'|\theta)$.
Initialise: $\theta_1 \sim P(\theta)$
for $j = 2$ to M **do**
  $\theta' \sim P(\theta'|\theta_{j-1})$ ▷ Sample proposed parameters
  $W \leftarrow \mathcal{M}(\theta')$ ▷ Run the bootstrap filter (algorithm 1) at θ'
  $\hat{\ell}(\theta') =\leftarrow \frac{1}{T}\sum_{t=1}^{T} \log \bar{W}_{\cdot,t}$ ▷ Calculate log-likelihood estimate (equation 2)
  $\alpha \leftarrow \min\left(\frac{\exp \hat{\ell}(\theta')}{\exp \hat{\ell}(\theta)} \frac{P(\theta')}{P(\theta_{j-1})} \frac{P(\theta|\theta')}{P(\theta'|\theta)}, 1\right)$ ▷ Calculate acceptance probability
  if $U \sim \text{Uniform}(0, 1) < \alpha$ **then**
    $\theta_j \leftarrow \theta'$ ▷ Accept the proposal
  else
    $\theta_j \leftarrow \theta_{j-1}$ ▷ Reject the proposal
  end if
end for
Return: Sampled parameter values $\{\theta_j\}_{j=1}^{M}$.

Practical considerations

To enable the calculation of convergence diagnostics, multiple (say, 4) chains of the PMMH algorithm should be run. We also encourage discarding an initial portion of each chain as a wind-in period. Diagnostics used in the examples below are the Gelman-Rubin statistic $\hat{R}$ [32] and effective sample size (ESS) [31], which are output by standard MCMC-analysis software. We use the MCMCChains.jl package [33] in our examples.

The standard Metropolis-Hastings algorithm uses exact evaluations of the model log-likelihood $\ell(\theta)$, whereas algorithm 1 admits a stochastic estimator $\hat{\ell}(\theta)$. The standard deviation of this estimator is a function of the number of particles N used in the bootstrap filter. It has been shown that the optimal standard deviation of $\hat{\ell}(\theta)$ is 1.2-1.3 [34, 35], which can be used to guide the choice of N. In practice, more likely values of θ result in a decreased standard deviation of $\hat{\ell}(\theta)$, so we aim to choose N such that the standard deviation of $\hat{\ell}(\theta)$ less than 1. For all examples in this primer, we use $N = 1000$ particles when estimating model likelihoods. We also note that, while larger standard deviations of $\hat{\ell}(\theta)$ result in slower convergence, model outputs are still valid.

The efficiency of the PMMH algorithm depends on the parameter proposal distribution $P(\theta'|\theta)$. We find that the heuristic multivariate Gaussian proposal distribution with covariance matrix $\Sigma = (2.38^2/d)\hat{\Sigma}$, where $\hat{\Sigma}$ is the sample covariance matrix of previous samples and d is the number of parameters being fit, generally performs well [36].

In the examples presented in this primer, we begin the PMMH algorithm with a diagonal covariance matrix and update this every 100 iterations until it stabilises (once $|\Sigma|$ changes by less than 20% between iterations), and then begin the primary sampling. Primary sampling is also performed in chunks of 100 samples, with the $\hat{R}$ and ESS calculated at the end of each chunk. We stop the algorithm when $\hat{R} < 1.05$ and ESS > 100 for all parameters. Complete details of these procedures are provided in the model files in the GitHub repository.

4 General framework

Thus far we have developed an algorithm for estimating the posterior distribution of hidden states X_t given observed data $y_{1:T}$ and parameter(s) θ, and an algorithm for estimating the posterior distribution of θ given $y_{1:T}$. In this section we demonstrate how these two algorithms can be used to perform inference and prediction.

4.1 Robust hidden state inference

We can couple the two algorithms to estimate the marginal smoothing distribution $P(X_t|y_{1:T})$, representing our beliefs about X_t while accounting for uncertainty about θ. Intuitively, we use the bootstrap filter to fit the model at multiple parameter samples $\theta^{(i)} \sim P(\theta|y_{1:T})$ and average the results:

$$\begin{aligned} P(X_t|y_{1:T}) &= E_{\theta|y_{1:T}}\left[P(X_t|y_{1:T},\theta)\right] \\ &\approx \frac{1}{N}\sum_{j=1}^{N} P(X_t|y_{1:T},\theta^{(j)}) \quad \text{where} \quad \theta^{(j)} \sim P(\theta|y_{1:T}) \end{aligned} \tag{5}$$

In practice, this is achieved by sampling N_θ parameter samples from the output of the PMMH algorithm (algorithm 2), and run the bootstrap filter (algorithm 1) at each of these samples. N particles are used in each bootstrap filter, resulting in a total of $N_\theta N$ particles approximating the marginal smoothing posterior. In the examples below, we use $N = 1,000$ and $N_\theta = 100$.

Algorithm 3 Marginal smoothing distribution sampler The bootstrap filter $\mathcal{M}$ written here accepts parameters θ_j and returns a matrix of hidden-state values.

1: **Input:** Number of PMMH parameter samples N_θ, unique parameter samples N_m, target posterior samples N_p, bootstrap filter $\mathcal{M}$.
2: **Initialise:** Pre-allocate matrix X of size $N_p \times T$.
3: Sample $\{\theta_j\}_{j=1}^{N_\theta}$ using algorithm 2.
4: **for** $i = 1, \ldots, N_m$ **do**
5: $\quad \theta \sim \{\theta_j\}_{j=1}^{N_\theta}$ ▷ Sample a parameter value
6: $\quad inds \leftarrow \{(i-1)N_m + 1, \ldots, iN_m\}$ ▷ Specify the indices of the ith block of X
7: $\quad X_{inds,\cdot} \leftarrow \mathcal{M}(\theta)$ ▷ Run the bootstrap filter (algorithm 1) at θ
8: **end for**

4.2 Prediction

Thus far we have focussed on model inference, both for hidden states X_t and parameter(s) θ. We may also be interested in making predictions about missing data Y_t, future data Y_{T+k}, or future hidden states X_{T+k}.

Predictive posterior distribution of observed data

The predictive posterior distribution of observed data is given by:

$$\begin{aligned} P(Y_t|y_{1:T}) &= E_{X_t|y_{1:T}}\left[P(Y_t|X_{1:t}, y_{1:T})\right] \\ &\approx \frac{1}{N}\sum_{j=1}^{N} P(Y_t|X_{1:t}, y_{1:T}) \quad \text{where} \quad X_{1:t} \sim P(X_t|y_{1:T}) \end{aligned} \tag{6}$$

In practice, we sample from the predictive posterior distribution by sampling N particles from the marginal smoothing distribution $x_{1:t}^{(i)} \sim P(X_{1:t}|y_{1:T})$ (the output of algorithm 3) and sampling a corresponding observation from $P(Y_t|x_{1:t}^{(i)}, y_{1:T})$ for each. The posterior predictive distribution can be calculated at any time step for which we have samples of hidden states, irrespective of whether data were observed on that time step.

Missing data

Missing data can be handled in a variety of ways depending on the type of missingness (missing at random, missing not at random, etc). Where data are missing by design (for example, wastewater sampling data may only be collected on certain days [21]), the observation distribution becomes $P(y_t \text{ is missing}|X_{1:t}, y_{1:t-1}, \theta) = 1$, irrespective of the values of the hidden states. In practice, we also skip the resampling step in the bootstrap filter on such days, as all hidden states are equally likely. More complex models, where the relationship between hidden states and missingness is explicitly modelled, are also possible. Prediction of missing data can be made by sampling from the observation model conditional on the value of the hidden states.

Forecasting

The projection of future hidden states (such as forecasting R_t) is handled similarly, effectively treating future data as missing by design, and projecting X_T forward by repeatedly sampling from the state-space transition distribution, producing forecasts of hidden states X_{T+k}. Forecasts of observed data Y_{T+k} can then be made by sampling from the observation distribution conditional on the forecasted hidden states.

Probability of elimination

Elimination of an infectious disease is defined as "the reduction to zero incidence of a certain pathogen in a given area" [37]. For the purposes of this primer, we say that elimination has occurred if no new infections occur within the next 28 days (an appropriate window for the SARS-CoV-2 examples we consider), although a variety of other definitions are possible [22]. This turns the problem of estimating the probability of elimination into a forecasting problem: we forecast the number of new infections in the next 28 days, and the proportion of particle trajectories that feature zero new infections provide an estimate of the probability of elimination.

4.3 Model evaluation and selection

Model evaluation and selection is a crucial component of any modelling exercise. We outline three tools: root-mean-square error (RMSE) of the posterior predictive distribution, the coverage of posterior predictive credible intervals, and the continuous ranked probability score (CRPS) [38] of the posterior predictive distribution.

The RMSE of the posterior predictive distribution is a measure of the average discrepancy between observed data and the model's predictions. It is calculated as:

$$\text{RMSE} = \sqrt{\frac{1}{T}\sum_{t=1}^{T}(y_t - \hat{y}_t)^2} \tag{7}$$

where $\hat{y}_t = E[Y_t|y_{1:T}]$ is the expected value of the posterior predictive distribution at time t.

The coverage of posterior predictive credible intervals is a measure of the proportion of observed data that falls within the model's credible intervals. It is calculated as:

$$\text{Coverage}_\alpha = \frac{1}{T}\sum_{t=1}^{T}\mathbb{I}(y_t \in \text{CI}_{\alpha,t}) \tag{8}$$

where $\text{CI}_{\alpha,t}$ is the α-level credible interval of the posterior predictive distribution at time t.

Finally, the CRPS of the posterior predictive distribution is a measure of the average discrepancy between the empirical CDF and the posterior CDF. It is defined as:

$$\text{CRPS} = \frac{1}{T}\sum_{t=1}^{T}\left(\int_{-\infty}^{\infty}(P(Y_t \leq y|y_{1:T}) - \mathbb{I}(y_t \leq y))^2 dy\right) \tag{9}$$

In practice, we use a particle approximation to the expectation-definition of the CRPS:

$$\begin{aligned} \text{CRPS} &= \frac{1}{T}\sum_{t=1}^{T}\left[\frac{1}{2}E|Y_t - Y_t'| - E|Y_t - y|\right] \quad \text{where} \quad Y_t, Y_t' \sim P(Y_t|y_{1:T}) \\ &\approx \frac{1}{T}\sum_{t=1}^{T}\left[\frac{1}{2}\frac{1}{N^2}\sum_{j=1}^{N}\sum_{k=1}^{N}|Y_t^{(j)} - Y_t^{(k)}| - \frac{1}{N}\sum_{j=1}^{N}|Y_t^{(j)} - y_t|\right] \end{aligned} \tag{10}$$

where $Y_t^{(j)}$ are samples from the posterior predictive distribution at time t. While all samples could be used, we find that a random subset of 100 samples per time step are sufficient, and lead to much faster computation times. The CRPS is particularly useful in the model selection process, as it provides a principled trade-off between model precision (such as RMSE) and calibration (such as coverage).

5 Example: COVID-19 in Aotearoa New Zealand

We demonstrate these methods on multiple models fit to national data from the COVID-19 pandemic in Aotearoa New Zealand [39]. Two time-periods are considered: 26 February 2020 - 4 June 2020 and 1 April 2024 - 9 July 2024. The former is characterised by a single epidemic wave with high quality case reporting and a large proportion of imported cases, during which elimination was the primary public health policy aim. The latter is characterised by widespread transmission with a clear day-of-the-week effect and high levels of reporting noise and bias, with modelling primarily used to inform health-service resource allocation.

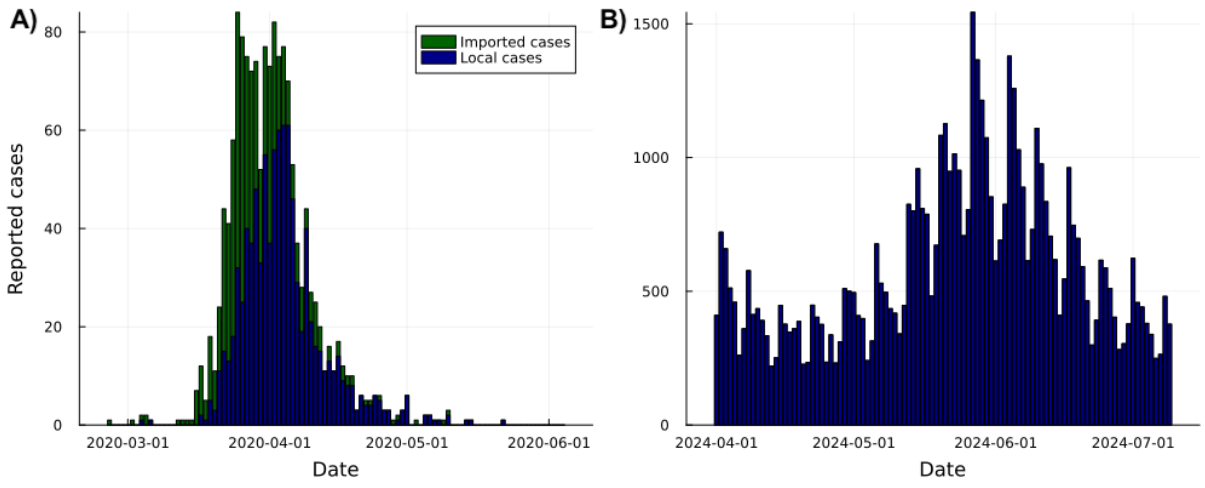

Figure 4: Reported cases from the COVID-19 pandemic in Aotearoa New Zealand, separated by locally-acquired and imported infections, for two time-periods: (A) 26 February 2020 - 4 June 2020 and (B) 1 April 2024 - 9 July 2024 [39]. The first period is the first wave of COVID-19 in Aotearoa New Zealand, characterised by a single epidemic wave which ended in elimination. The second period is characterised by widespread transmission with much higher numbers of reported cases.

5.1 A simple example

As a first example, we implement a model very similar to EpiFilter [5], assuming that R_t follows a log-normal random walk (the state-space transition model):

$$\log R_t | \log R_{t-1} \sim \text{Normal}(\log R_{t-1}, \sigma) \tag{11}$$

and observed cases follow the Poisson renewal model (the observation model):

$$C_t | R_t, C_{1:t-1} \sim \text{Poisson}\left(R_t \sum_{u=1}^{u_{max}} C_{t-u}\omega_u\right) \tag{12}$$

The hidden states are given by $X_t = R_t$, the observed data by $y_t = C_t$, and parameters by $\theta = \sigma$. We could additionally consider the serial interval $\omega_u, u = 1, \ldots$ as model parameters, but for simplicity we assume this is part of the model structure, a typical assumption in such models.

First we use PMMH (algorithm 2) to estimate the posterior distribution of σ. Assuming a uniform prior distribution on $(0, 1)$, we find a posterior mean of 0.24 (95% Credible Interval (Cr. I) 0.16, 0.34). Convergence (in this case, $\hat{R} = 1.001$ and ESS = 126) was obtained in 200 iterations, taking approximately 10 seconds on a 2021 M1 MacBook Pro.

The focus of this example is on hidden-state inference: the estimation of R_t. We produce estimates of daily R_t and corresponding 95% credible intervals using algorithm 3, effectively averaging over the posterior uncertainty about σ. These estimates are shown in panel A of figure 5.

We also present the posterior predictive distribution of reported cases in figure 5-B. By comparing observed data to these posterior predictive intervals, we can assess the calibration of the reported credible intervals. In this case, the model fits the data well, with 97.9% of observed cases falling inside the daily 95% posterior predictive credible intervals.

By halting the SMC algorithm on 5 April 2020 and using $L = 30$ as the resampling lag, we can generate samples from the joint marginal distribution $P(R_{7 \text{ March:5 April}} | C_{1:T})$, presented in figure 5-C. These samples allow us to estimate the joint posterior distribution of the epidemic peak and the timing of this peak. This is reported as a heatmap of the log-posterior density in figure 5-D, where brighter colours represent more likely combinations of these values. The marginal posterior distributions of peak R_t and the date of the peak are shown in panels E and F of figure 5. We estimate that R_t peaked at 6.7 (95% Cr.I 4.8, 9.7) on median 17 March 2020 (95% Cr.I 15 March, 22 March).

Two distinct modes can be seen in the log-posterior density heatmap: one with a peak on 17 March 2020 and the other with a peak on 22 March 2020. The peak on 17 March is associated with a higher value of 7.1 (5.1, 10.2) (if we condition on this peak date), while a peak on 22 March 2020 is estimated to be lower, at 5.7 (4.6, 7.1).

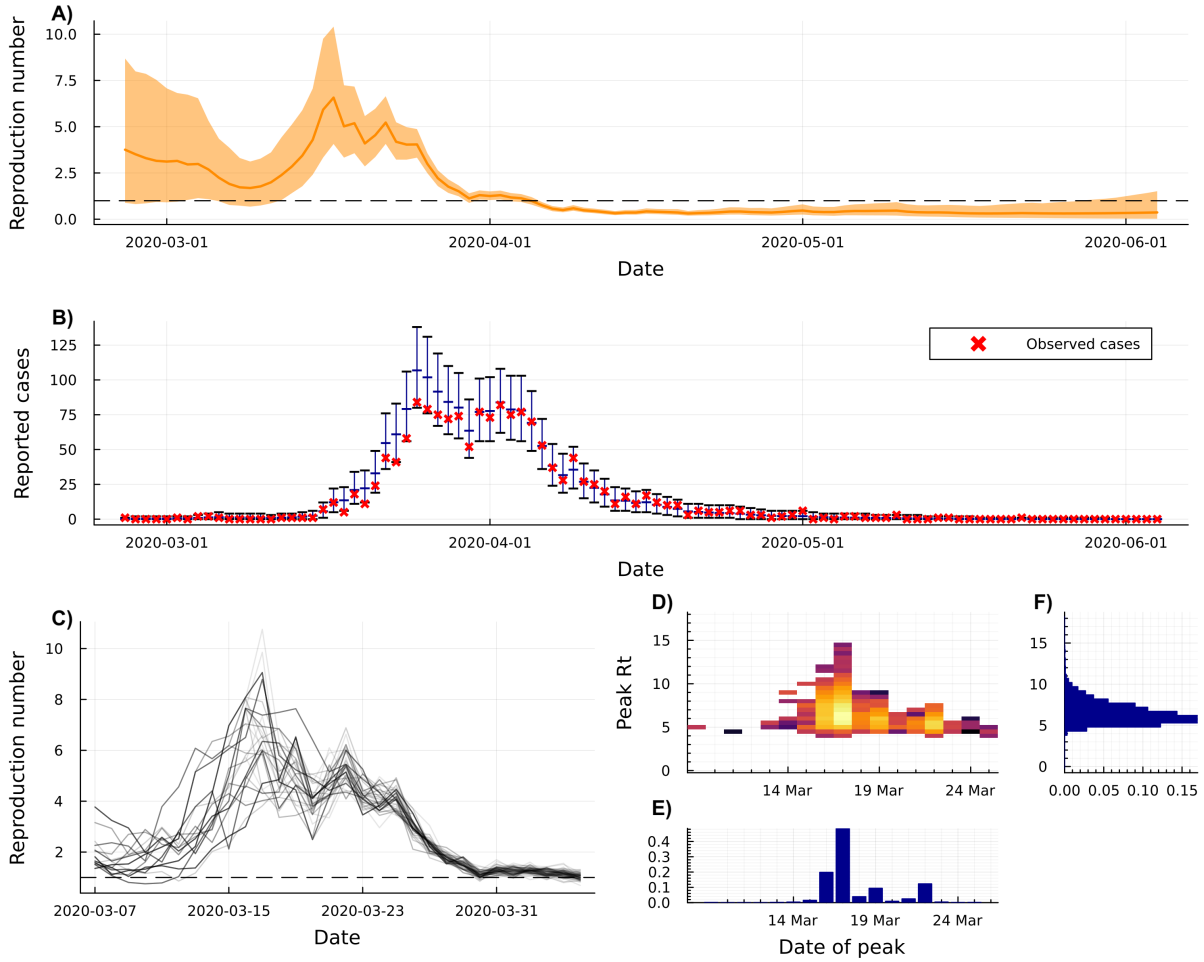

Figure 5: Model results from the simple example. The marginal posterior mean and 95% credible intervals of R_t (panel A) demonstrates high uncertainty in the early stages as well as a high peak estimate of R_t in late-March 2020. The marginal posterior predictive distribution of reported cases (panel B) shows that the model fits the data well, with the majority of the observed cases falling inside the 95% posterior predictive credible interval. Panel (C) shows equally-likely samples from the joint posterior distribution of R_t between 7 March and 5 April 2020. These samples can be used to find the joint posterior distribution of peak R_t and the date of this peak, reported as a log-density heatmap (panel D), where brighter colours represent more likely combinations of these values. The marginal posterior distributions of peak R_t and the date of the peak are shown in panels E and F, respectively. Panels (D-E) suggest that the peak was most likely around 17 March 2020, although a second mode is visible with lower peak R_t on 22 March 2020.

5.2 Reporting noise, imported cases and elimination probabilities

Surveillance of COVID-19 in Aotearoa New Zealand was generally considered to be of high quality, although it is still desirable to account for certain known biases. Firstly, we acknowledge that infection incidence is not directly observed. Instead, we observe reported cases which are subject to reporting noise. Secondly, a large proportion of reported cases in the early phase of the pandemic in New Zealand were imported cases, those infected outside of New Zealand. If these are not properly accounted for, the model may overestimate R_t as it attributes these cases to local transmission. During this time, elimination of SARS-CoV-2 was an explicit public-health policy goal in New Zealand. Models explicitly estimating the probability of elimination were of key interest to policy-makers, particularly as repeated days of zero cases were observed. We

demonstrate how our methods can be used to estimate the probability of elimination, defined here as the probability that $I_{t:t+28} = 0$, while simultaneously accounting for reporting noise and imported cases.

We model infection incidence as a new hidden state, which is assumed to evolve according to the renewal model. The expected number of local infections I_t at time t is a function of R_t, the serial interval ω_u, past local infections $I_{1:t-1}$, and past imported cases $M_{1:t-1}$:

$$\begin{aligned} \log R_t | \log R_{t-1} &\sim \text{Normal}(\log R_{t-1}, \sigma) \\ I_t | R_t, I_{1:t-1} &\sim \text{Poisson}\left(R_t \sum_{u=1}^{u_{max}} (I_{t-u} + M_{t-u})\omega_u\right) \end{aligned} \tag{13}$$

we then assume that reported cases C_t follow a Negative Binomial distribution with mean I_t and variance $I_t + \phi I_t^2$:

$$C_t | I_{1:t-1} \sim \text{Negative Binomial}\left(r = \frac{1}{\phi}, p = \frac{1}{1 + \phi I_t}\right) \tag{14}$$

The parameter ϕ controls the level of observation noise, which we estimate alongside σ using PMMH. Like σ, we use a uniform prior distribution on $(0, 1)$ for ϕ.

Using PMMH (algorithm 2) we estimate a posterior mean and 95% credible interval of σ of 0.18 (0.12, 0.26) and ϕ of 0.014 (0.0003, 0.059). The decreased estimate of σ reflects the re-attribution of some noise in the data to the observation process, rather than the epidemic process. The estimate of ϕ is low, suggesting that the observation process may be adequately modelled by a Poisson distribution, instead of the Negative Binomial distribution we have assumed (this could be tested using the model selection metrics outlined in section 4.3). Convergence was obtained in 600 iterations, taking approximately 30 seconds on a 2021 M1 MacBook Pro.

Daily posterior means and 95% credible intervals of R_t are reported in figure 6-A. Despite being fit to data from the same outbreak as the simple example, the estimates of R_t are very different. By halting the algorithm on 5 April 2020, we estimate that R_t peaked at 1.7 (1.2, 2.4) on 23 March 2020 (17 March, 27 March), much lower and later than estimates from the simple model. This decrease is primarily a result of distinguishing locally-acquired from imported cases, although the re-attribution of noise from the epidemic process to the observation process also plays a role.

Figure 6-B demonstrates that the model fits the data well, although the fact that 100% of observed cases fall inside the 95% posterior predictive credible intervals suggests that we may be allowing for too much observation noise. Plotting the histogram of samples of ϕ suggests that $\phi = 0$ (i.e. Poisson observation noise) is a plausible value, upon which the uniform prior distribution places very little mass.

The probability of elimination (defined as the probability that no new local infections occur within the next 28 days, conditional on no new imported cases) increases steadily from early Mary and is estimated to reach 84.3% on the final time step 4 June 2020. Conditioning on no new imported cases is equivalent to assuming that any imported infections cause no local transmission, a reasonable assumption given the strict border controls in place at the time.

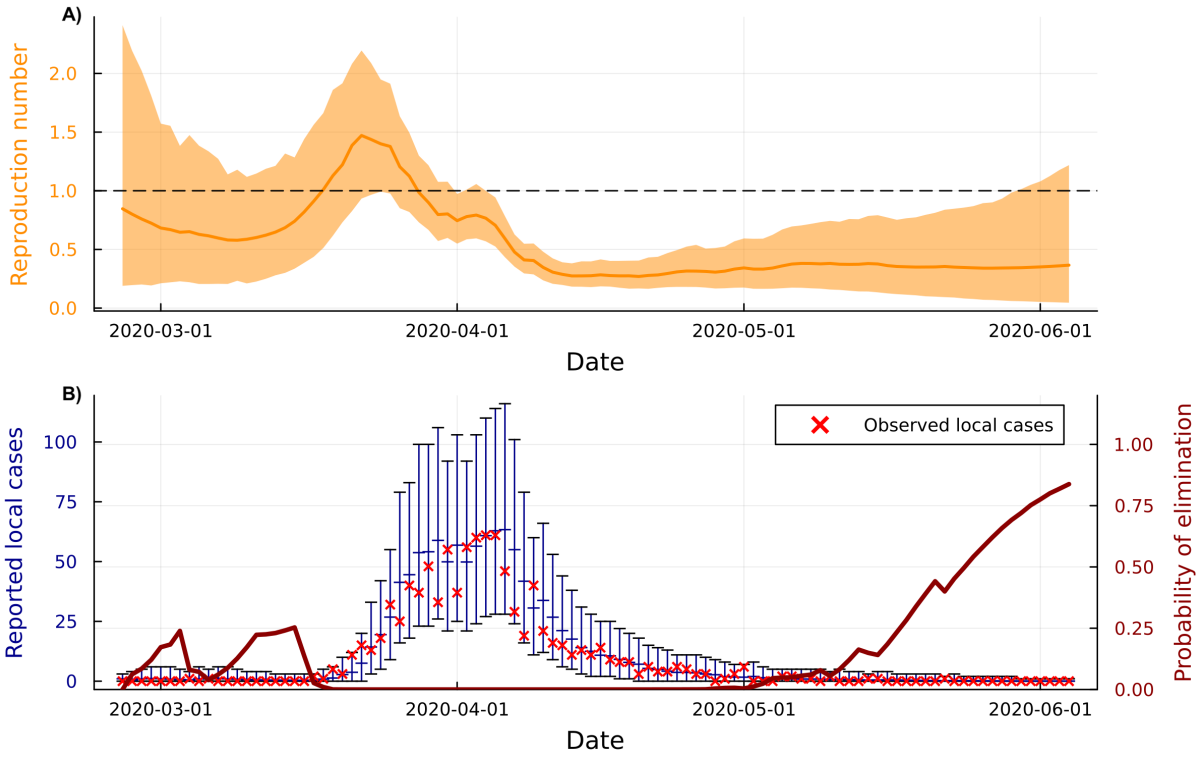

Figure 6: Model results when accounting for reporting noise and imported cases. The marginal posterior mean and 95% credible intervals of R_t (panel A) demonstrate a much lower and somewhat later peak in March 2020 than the simple model, reflecting the re-attribution of noise to the observation process and the distinction between locally-acquired and imported cases. The marginal posterior predictive distribution of reported cases (panel B) shows that the model fits the observed data well, with observed data often lying close to posterior predictive means. The probability of elimination increases steadily from early May and is estimated to reach 84.3% on the final time step 4 June 2020.

5.3 Reporting biases, temporal effects and forecasting

For the final example we consider reported cases of COVID-19 in New Zealand between 1 April 2024 and 9 July 2024, a period characterised by widespread transmission, decreased testing rates, and increased reporting delays and noise. A clear day-of-the-week effect can be observed in the reported case data, with fewer cases reported on weekends. This can be accounted for by explicitly including a day-of-the-week effect or by modelling temporally aggregated data. We demonstrate both here.

We use a similar state-space transition model as the previous example, although ignore imported cases for simplicity:

$$\begin{aligned} \log R_t | \log R_{t-1} &\sim \text{Normal}(\log R_{t-1}, \sigma) \\ I_t | R_t, I_{1:t-1} &\sim \text{Poisson}\left(R_t \sum_{u=1}^{u_{max}} I_{t-u}\omega_u\right) \end{aligned} \tag{15}$$

To account for reporting delays, the expected number of cases μ_t at time t is modelled as a function of past incidence $I_{1:t-1}$ and an incubation distribution d_u, assumed to be Gamma-distributed with mean 5.5 days and standard deviation 2.3 days:

$$\mu_t = \sum_{u=1}^{u_{max}} I_{t-u} d_u \tag{16}$$

For the day-of-the-week model, we introduce seven new parameters: $c_i, i = 1, \ldots, 7$, representing the relative reporting rate on day i. These parameters are subject to the constraint that $\sum_{i=1}^{7} c_i = 7$, enforced by estimating $c_1, \ldots, c_6$ and setting $c_7 = 7 - \sum_{i=1}^{6} c_i$. The observation distribution in this case is given by:

$$C_t | \mu_t, \phi \sim \text{Negative Binomial}\left(r = \frac{1}{\phi}, p = \frac{1}{1 + \phi c_{\text{mod}(t,7)+1} \mu_t}\right) \tag{17}$$

where $c_{\text{mod}(t,7)+1}$ is the day-of-the-week effect for day t.

For the weekly-aggregated model, we calculate particle weights and resample on a weekly basis. When $\text{mod}(t, 7) = 0$, we define $C'_t = \sum_{i=t-6}^{t} C_i$ as the weekly aggregated data, and the observation distribution is given by:

$$C'_t | \mu_{t-6:t}, \phi \sim \text{Negative Binomial}\left(r = \frac{1}{\phi}, p = \frac{1}{1 + \phi \sum_{i=t-6}^{t} \mu_i}\right), \quad \text{if mod}(t, 7) = 0 \tag{18}$$

Using PMMH (algorithm 2), we find that both models produce similar estimates of σ: 0.074 (0.043, 0.132) for the day-of-the-week model and 0.070 (0.039, 0.132) for the weekly-aggregated model. The models also produce somewhat similar estimates of ϕ: 0.011 (0.007, 0.015) for the day-of-the-week model and 0.008 (0.001, 0.038) for the temporally aggregated model. The similarity of the estimates of σ suggest that the format of the data does not substantially impact the estimated epidemiological dynamics, and the similarity of ϕ estimates suggests that, once the day-of-the-week effect has been accounted for, both data sources exhibit a similar level of overdispersion.

Figure 6-A presents the daily posterior mean and 95% credible intervals of R_t for both models. Both models produce similar estimates of R_t, although the weekly-aggregated model exhibits slightly more uncertainty, reflecting the decrease in information associated with the aggregation of data. The day-of-the-week model is able to capture the day-of-the-week effect, with 96.9% of observed cases falling inside the 95% posterior predictive credible intervals. Finally, all fourteen observations of weekly data fall inside the 95% posterior predictive credible intervals of the weekly-aggregated model.

Four-week forecasts are produced by iterating the state-space model forward and sampling from the observation model. In both models, 100% of future cases fall inside the 95% posterior predictive credible intervals, suggesting that the models are conservative in their uncertainty quantification, most likely a result of model misspecification.

It is also possible to ignore the day-of-week effect and fit a "naive" model with observation distribution:

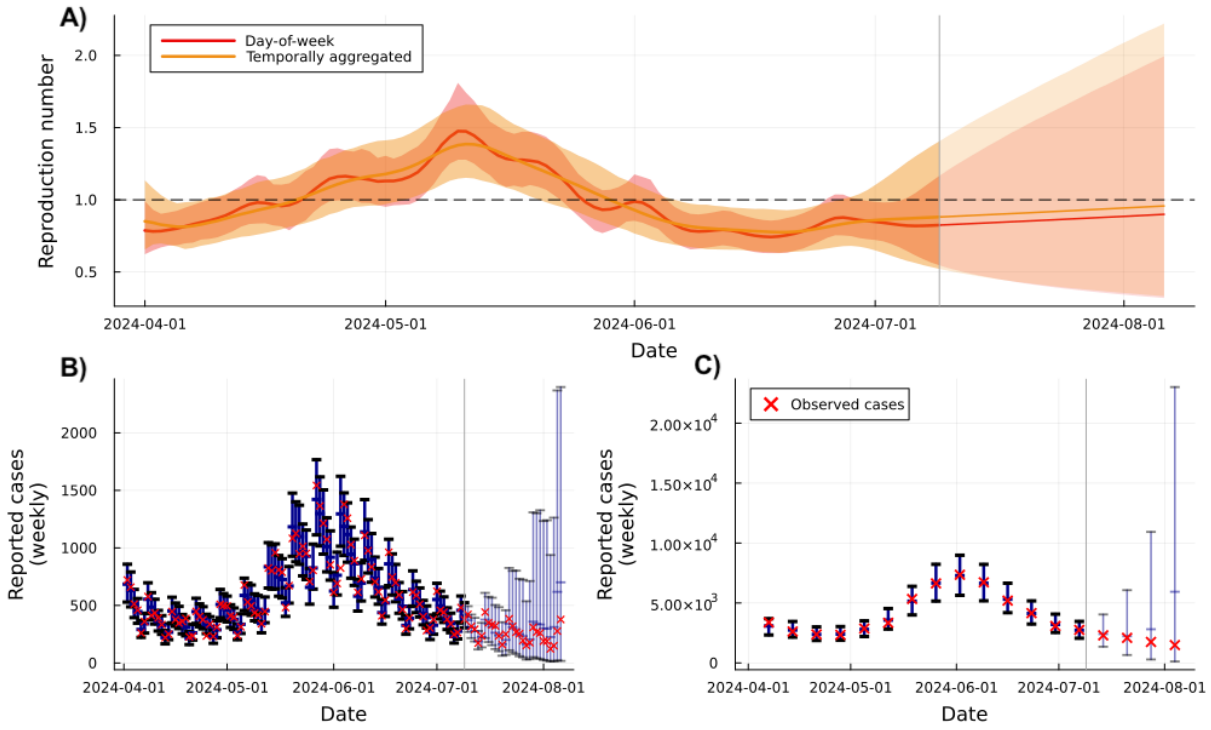

Figure 7: Model results when accounting for weekly administrative noise. The dark red line and shaded region presents the marginal posterior mean and 95% credible intervals of R_t for the day-of-the-week model, with estimates from the temporally aggregated model in orange (panel A). Predictive daily cases are shown in panel B, while predictive weekly aggregated cases are shown in panel C. Forecasts of R_t and reported cases are shown in all three panels, with lighter shading and the vertical gray bar marking the start of the forecast.

$$C_t|\mu_t, \phi \sim \text{Negative Binomial}\left(r = \frac{1}{\phi}, p = \frac{1}{1+\phi\mu_t}\right) \tag{19}$$

Corresponding estimates of R_t and predictive cases are reported in section 7 (supplementary figures). This model assumes the day of the week is noise arising from the negative binomial observation process, thus the estimate of ϕ is much greater than in the other models, with mean and Cr.I 0.0731 (0.0527, 0.0919). Despite this, reproduction number estimates from the naive model are similar to those from the temporally aggregated model, reflecting the similarity of the information content they leverage.

As we fit the naive model and the day-of-the-week model to the same data, we can compare the two models using RMSE and CRPS. The RMSE of the naive model is 5.4x greater than the day-of-the-week model on within-sample predictions and 255x greater on the 4-week forecasts, suggesting that the day-of-the-week model produces much more accurate central estimates. CRPS, which simultaneously accounts for calibration and precision, is 2.6x greater for the naive model on within-sample predictions and 1.53x greater on out-of-sample predictions. This suggests that the day-of-the-week model is substantially better than the naive model, despite the additional complexity and similarity of hidden-state estimates.

6 Discussion

We have introduced a general framework for fitting epidemic renewal models using SMC methods, and demonstrated how these methods can be used to estimate hidden states, estimate parameters, and make predictions. The primary strength of these methods is their flexibility: they can be used to fit any state-space model, a form in which many popular epidemiological models can be expressed.

We demonstrate our methods on three examples. Each example consists of a unique combination of model structure, data, and aims, yet the same general framework is used to fit each model. The first example demonstrates the estimation of R_t using a simple renewal model, similar to [5], except we additionally extract joint reproduction number trajectories, allowing us to jointly estimate the peak R_t value and timing of this peak. The second example demonstrates the estimation of R_t while simultaneously accounting for reporting noise [40, 41, 42, 43, 44] and imported cases [45], while also estimating the probability of elimination [22], thus unifying the cited works. The final example demonstrates the estimation of R_t in the presence of reporting delays [44] and day-of-the-week effects [46] or temporally aggregated data [26, 47, 48], as well as the ability to produce short-term forecasts [49], and the importance of model comparison and selection [6, 11], again unifying the cited (and many non-cited) works. Many other extensions are possible, particularly the ability to incorporate multiple data sources [21].

Many modelling choices made in our examples are arbitrary: for example, a Poisson observation distribution could be used in the second example (instead of a negative binomial distribution), the day-of-week-effect could be modelled as daily binomial reporting probabilities, and there are many ways to define elimination, to highlight just a few. Different researchers may choose to approach the same problem in different ways. The core strength of these methods is their ability to quickly and easily test these different models. We also provide principled methods for model evaluation and selection, including RMSE, CRPS, and coverage of posterior predictive credible intervals. While these metrics are useful for comparing models fit to the same underlying data, they are less useful for comparing models fit to different data sources, a potential area for future work.

Correctly accounting for uncertainty in model parameters has previously been shown to be critical for robust uncertainty quantification, and thus for robust decision-making [50]. Our focus on marginalising out uncertainty about model parameters is a key strength of these methods, and is a feature not present in many other epidemiological models, including many SMC-based approaches [22].

Epidemic models range from highly mechanistic (such as compartmental SIR-type models) to purely statistical (such as time-series regression, ARIMA models, and exponential smoothers). The renewal model is semi-mechanistic in that it imposes a simple structure but does not model the entire underlying process. This leads to a model that is flexible, interpretable, and can produce well-calibrated short-term forecasts. We also highlight, however, that the renewal model implies a specific autocorrelation structure in the data. If this structure is misspecified, and the only goal is the forecasting of observable data, then model may underperform compared to more flexible statistical models [6]. Some of this can be overcome by fitting more flexible observation models.

Our focus on simplicity and flexibility results in algorithms that are known to be less efficient than more complex approaches. Areas for improvement include the use of better-tuned particle proposal densities (in algorithm 1) [29], the use of more advanced resampling schemes (in algorithm 1) [51], and the use of better-tuned parameter proposal densities (in algorithm 2) [34, 52]. Many solutions to these problems exist within the literature, often leveraging specific details about the chosen model, and we encourage the reader to seek out more efficient algorithms once a model is constructed. In addition to the epidemiology-specific literature [23, 24], we also recommend two books from the broader SMC literature [10, 51].

An effective alternative to SMC-type methods for performing inference and prediction with epidemic renewal models are probabilistic-programming-language-based Gaussian process approximations, such as EpiNow2 [4]. These methods feature a similar level of flexibility and, in some cases, can be faster than our approach. However, these methods are more complex mathematically, where ours can are more accessible to those with a less mathematical background and can be implemented in a few lines of code.

One limitation of our framework (and of state-space models in general) is that we assume y_t is fully observed at time t and will not change in the future. In epidemiology, this is often not the case, as data are frequently revised and updated, necessitating the use of nowcasting methods [53, 11]. It is not immediately obvious how to incorporate this into our framework (other than to not update past data), and is probably the largest limitation of our methods.

Numerous methods for estimating R_t and conducting inference on epidemic data exist, often tailored to specific cases. More general models have also been created, although these are often challenging to implement, or are confined to pre-built software packages. While these such packages simplify the process, they can obscure the model's underlying structure and assumptions. This primer aims to strike a balance: enabling researchers to quickly and easily construct their own models from scratch, ensuring they understand the assumptions and structure of the model, while facilitating rapid testing and comparison of different models.

7 Supplementary figures

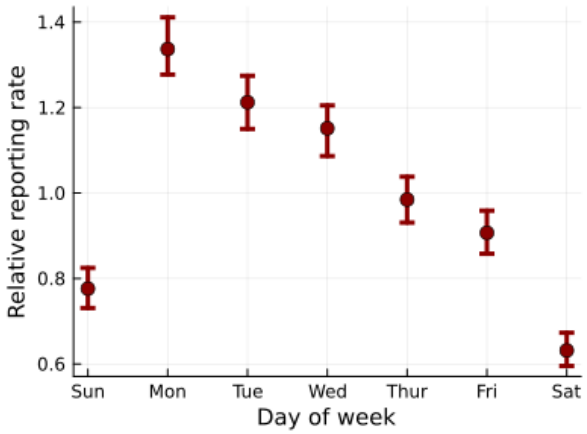

Figure 8: Estimated model parameters c_i for $i = 1 \dots 7$ from the day-of-the-week model, giving estimates of the relative reporting rate on each day of the week.

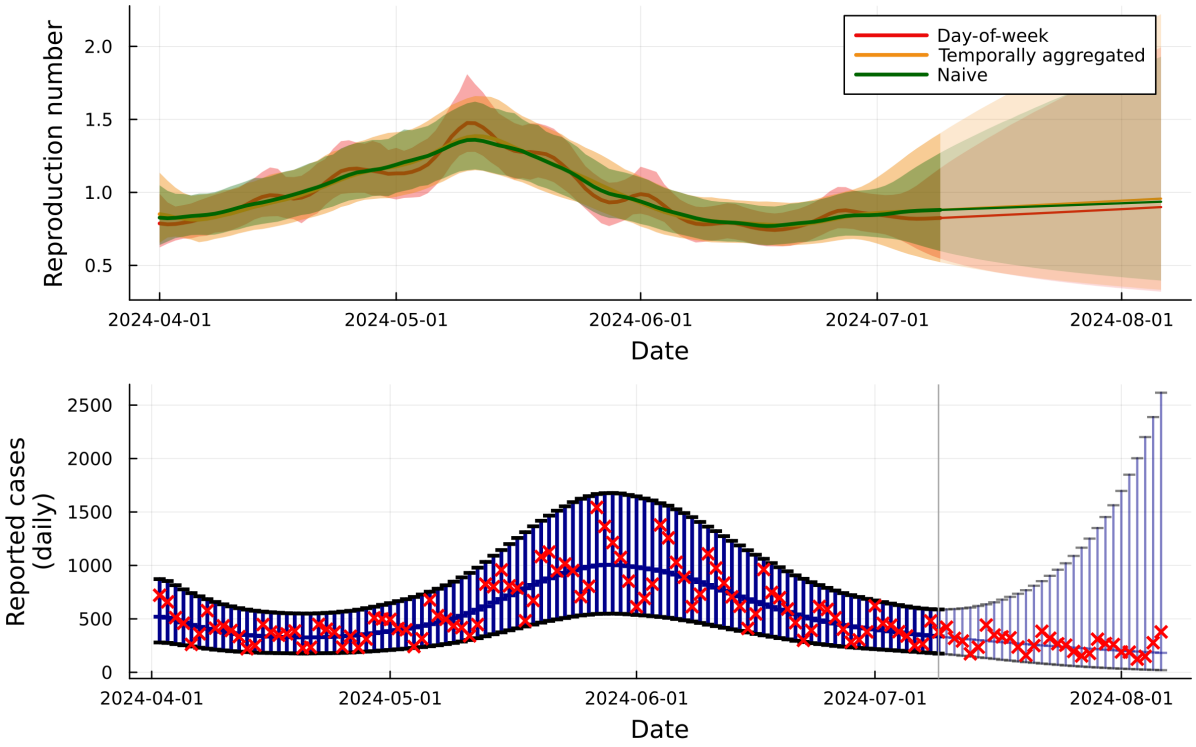

Figure 9: Model results when not accounting for weekly administrative noise (dark green R_t) and reported cases.

References

[1] Joseph A Lewnard and Arthur L Reingold. "Emerging Challenges and Opportunities in Infectious Disease Epidemiology". In: *American Journal of Epidemiology* 188.5 (May 2019), pp. 873–882. ISSN: 0002-9262. DOI: 10.1093/aje/kwy264. (Visited on 10/04/2024).

[2] Christophe Fraser. "Estimating Individual and Household Reproduction Numbers in an Emerging Epidemic". In: *PLoS ONE* 2.8 (Aug. 2007). Ed. by Alison Galvani, e758. ISSN: 1932-6203. DOI: 10.1371/journal.pone.0000758. (Visited on 10/04/2024).

[3] Anne Cori et al. "A New Framework and Software to Estimate Time-Varying Reproduction Numbers During Epidemics". In: *American Journal of Epidemiology* 178.9 (Nov. 2013), pp. 1505–1512. ISSN: 0002-9262. DOI: 10.1093/aje/kwt133. (Visited on 09/09/2023).

[4] Sam Abbott et al. "Estimating the Time-Varying Reproduction Number of SARS-CoV-2 Using National and Subnational Case Counts". In: *Wellcome Open Research* 5 (Dec. 2020), p. 112. ISSN: 2398-502X. DOI: 10.12688/wellcomeopenres.16006.2. (Visited on 09/09/2023).

[5] Kris V. Parag. "Improved Estimation of Time-Varying Reproduction Numbers at Low Case Incidence and between Epidemic Waves". In: *PLOS Computational Biology* 17.9 (Sept. 2021), e1009347. ISSN: 1553-7358. DOI: 10.1371/journal.pcbi.1009347. (Visited on 09/10/2023).

[6] Nicolas Banholzer et al. *A Comparison of Short-Term Probabilistic Forecasts for the Incidence of COVID-19 Using Mechanistic and Statistical Time Series Models*. May 2023. DOI: 10.48550/arXiv.2305.00933. arXiv: 2305.00933 [cs, q-bio, stat]. (Visited on 09/15/2024).

[7] Kris V. Parag, Benjamin J. Cowling, and Christl A. Donnelly. "Deciphering Early-Warning Signals of SARS-CoV-2 Elimination and Resurgence from Limited Data at Multiple Scales". In: *Journal of The Royal Society Interface* 18.185 (Dec. 2021), p. 20210569. ISSN: 1742-5662. DOI: 10.1098/rsif.2021.0569. (Visited on 10/03/2024).

[8] Seth Flaxman et al. "Estimating the Effects of Non-Pharmaceutical Interventions on COVID-19 in Europe". In: *Nature* 584.7820 (Aug. 2020), pp. 257–261. ISSN: 1476-4687. DOI: 10.1038/s41586-020-2405-7. (Visited on 04/17/2024).

[9] Rebecca K. Nash, Pierre Nouvellet, and Anne Cori. "Real-Time Estimation of the Epidemic Reproduction Number: Scoping Review of the Applications and Challenges". In: *PLOS Digital Health* 1.6 (June 2022), e0000052. ISSN: 2767-3170. DOI: 10.1371/journal.pdig.0000052. (Visited on 09/04/2024).

[10] Arnaud Doucet, Nando De Freitas, and Neil Gordon, eds. *Sequential Monte Carlo Methods in Practice*. Statistics for Engineering and Information Science. New York: Springer, 2001. ISBN: 978-0-387-95146-1.

[11] Katelyn M. Gostic et al. "Practical Considerations for Measuring the Effective Reproductive Number, Rt". In: *PLOS Computational Biology* 16.12 (Dec. 2020), e1008409. ISSN: 1553-7358. DOI: 10.1371/journal.pcbi.1008409. (Visited on 09/12/2023).

[12] Chenguang Dai et al. "An Invitation to Sequential Monte Carlo Samplers". In: *Journal of the American Statistical Association* 117.539 (July 2022), pp. 1587–1600. ISSN: 0162-1459, 1537-274X. DOI: 10.1080/01621459.2022.2087659. (Visited on 10/03/2024).

[13] Anahita Safarishahrbijari et al. "Predictive Accuracy of Particle Filtering in Dynamic Models Supporting Outbreak Projections". In: *BMC Infectious Diseases* 17.1 (Sept. 2017), p. 648. ISSN: 1471-2334. DOI: 10.1186/s12879-017-2726-9. (Visited on 09/02/2024).

[14] Xiaoyan Li et al. "Real-Time Epidemiology and Acute Care Need Monitoring and Forecasting for COVID-19 via Bayesian Sequential Monte Carlo-Leveraged Transmission Models". In: *International Journal of Environmental Research and Public Health* 21.2 (Feb. 2024), p. 193. ISSN: 1660-4601. DOI: 10.3390/ijerph21020193. (Visited on 10/03/2024).

[15] Jessica Welding and Peter Neal. *Real Time Analysis of Epidemic Data*. Sept. 2019. DOI: 10.48550/arXiv.1909.11560. arXiv: 1909.11560 [stat]. (Visited on 10/03/2024).

[16] Geir Storvik et al. "A Sequential Monte Carlo Approach to Estimate a Time-Varying Reproduction Number in Infectious Disease Models: The Covid-19 Case*". In: *Journal of the Royal Statistical Society Series A: Statistics in Society* 186.4 (Oct. 2023), pp. 616–632. ISSN: 0964-1998. DOI: 10.1093/jrsssa/qnad043. (Visited on 10/03/2024).

[17] Daniel M. Sheinson, Jarad Niemi, and Wendy Meiring. "Comparison of the Performance of Particle Filter Algorithms Applied to Tracking of a Disease Epidemic". In: *Mathematical Biosciences* 255 (Sept. 2014), pp. 21–32. ISSN: 0025-5564. DOI: 10.1016/j.mbs.2014.06.018. (Visited on 10/03/2024).

[18] Yong Sul Won et al. "Estimating the Instantaneous Reproduction Number (Rt) by Using Particle Filter". In: *Infectious Disease Modelling* 8.4 (Dec. 2023), pp. 1002–1014. ISSN: 2468-0427. DOI: 10.1016/j.idm.2023.08.003. (Visited on 09/02/2024).

[19] Wan Yang, Alicia Karspeck, and Jeffrey Shaman. "Comparison of Filtering Methods for the Modeling and Retrospective Forecasting of Influenza Epidemics". In: *PLOS Computational Biology* 10.4 (Apr. 2014), e1003583. ISSN: 1553-7358. DOI: 10.1371/journal.pcbi.1003583. (Visited on 10/03/2024).

[20] Lorenzo Rimella, Christopher Jewell, and Paul Fearnhead. *Approximating Optimal SMC Proposal Distributions in Individual-Based Epidemic Models*. Mar. 2023. DOI: 10.48550/arXiv.2206.05161. arXiv: 2206.05161 [stat]. (Visited on 10/03/2024).

[21] Leighton M. Watson et al. "Jointly Estimating Epidemiological Dynamics of Covid-19 from Case and Wastewater Data in Aotearoa New Zealand". In: *Communications Medicine* 4.1 (July 2024), pp. 1–9. ISSN: 2730-664X. DOI: 10.1038/s43856-024-00570-3. (Visited on 09/02/2024).

[22] M. J. Plank et al. *Robust Estimation of End-of-Outbreak Probabilities in the Presence of Delayed and Incomplete Case Reporting*. Sept. 2024. DOI: 10.48550/arXiv.2409.16531. arXiv: 2409.16531. (Visited on 10/22/2024).

[23] Dhorasso Temfack and Jason Wyse. *A Review of Sequential Monte Carlo Methods for Real-Time Disease Modeling*. 2024. DOI: 10.48550/ARXIV.2408.15739. (Visited on 10/03/2024).

[24] Akira Endo, Edwin van Leeuwen, and Marc Baguelin. "Introduction to Particle Markov-chain Monte Carlo for Disease Dynamics Modellers". In: *Epidemics* 29 (Dec. 2019), p. 100363. ISSN: 1755-4365. DOI: 10.1016/j.epidem.2019.100363. (Visited on 09/10/2023).

[25] Christophe Fraser et al. "Influenza Transmission in Households During the 1918 Pandemic". In: *American Journal of Epidemiology* 174.5 (Sept. 2011), pp. 505–514. ISSN: 0002-9262. DOI: 10.1093/aje/kwr122. (Visited on 04/17/2024).

[26] I Ogi-Gittins et al. "Efficient Simulation-Based Inference of the Time-Dependent Reproduction Number from Temporally Aggregated and under-Reported Disease Incidence Time Series Data". In: *Work in progress* (2024).

[27] Anne Cori and Adam Kucharski. "Inference of Epidemic Dynamics in the COVID-19 Era and Beyond". In: *Epidemics* 48 (Sept. 2024), p. 100784. ISSN: 1755-4365. DOI: 10.1016/j.epidem.2024.100784. (Visited on 09/02/2024).

[28] N. J. Gordon, D. J. Salmond, and A. F. M. Smith. "Novel Approach to Nonlinear/Non-Gaussian Bayesian State Estimation". In: *IEE Proceedings F (Radar and Signal Processing)* 140.2 (Apr. 1993), pp. 107–113. ISSN: 2053-9045. DOI: 10.1049/ip-f-2.1993.0015. (Visited on 09/09/2023).

[29] Michael K. Pitt and Neil Shephard. "Filtering via Simulation: Auxiliary Particle Filters". In: *Journal of the American Statistical Association* 94.446 (1999), pp. 590–599. ISSN: 0162-1459. DOI: 10.2307/2670179. JSTOR: 2670179. (Visited on 10/25/2024).

[30] Christophe Andrieu, Arnaud Doucet, and Roman Holenstein. "Particle Markov Chain Monte Carlo Methods". In: *Journal of the Royal Statistical Society: Series B (Statistical Methodology)* 72.3 (2010), pp. 269–342. ISSN: 1467-9868. DOI: 10.1111/j.1467-9868.2009.00736.x. (Visited on 09/13/2023).

[31] Andrew Gelman. *Bayesian Data Analysis*. Third edition. Chapman & Hall/CRC Texts in Statistical Science. Boca Raton: CRC Press, 2014.

[32] Andrew Gelman and Donald B. Rubin. "Inference from Iterative Simulation Using Multiple Sequences". In: *Statistical Science* 7.4 (Nov. 1992), pp. 457–472. ISSN: 0883-4237, 2168-8745. DOI: 10.1214/ss/1177011136. (Visited on 10/25/2024).

[33] *MCMCChains*. 2024. (Visited on 10/25/2024).

[34] Nikolas Kantas et al. "On Particle Methods for Parameter Estimation in State-Space Models". In: *Statistical Science* 30.3 (Aug. 2015), pp. 328–351. ISSN: 0883-4237, 2168-8745. DOI: 10.1214/14-STS511. (Visited on 09/13/2023).

[35] A. Doucet et al. "Efficient Implementation of Markov Chain Monte Carlo When Using an Unbiased Likelihood Estimator". In: *Biometrika* 102.2 (June 2015), pp. 295–313. ISSN: 0006-3444. DOI: 10.1093/biomet/asu075. (Visited on 10/25/2024).

[36] Christophe Andrieu and Johannes Thoms. "A Tutorial on Adaptive MCMC". In: *Statistics and Computing* 18.4 (Dec. 2008), pp. 343–373. ISSN: 1573-1375. DOI: 10.1007/s11222-008-9110-y. (Visited on 10/25/2024).

[37] Petra Klepac et al. "Six Challenges in the Eradication of Infectious Diseases". In: *Epidemics*. Challenges in Modelling Infectious DIsease Dynamics 10 (Mar. 2015), pp. 97–101. ISSN: 1755-4365. DOI: 10.1016/j.epidem.2014.12.001. (Visited on 10/25/2024).

[38] Tilmann Gneiting and Adrian E Raftery. "Strictly Proper Scoring Rules, Prediction, and Estimation". In: *Journal of the American Statistical Association* 102.477 (Mar. 2007), pp. 359–378. ISSN: 0162-1459. DOI: 10.1198/016214506000001437. (Visited on 09/13/2024).

[39] Ministry of Health NZ. *New Zealand COVID-19 Data*. (Visited on 09/13/2024).

[40] Jana S Huisman et al. "Estimation and Worldwide Monitoring of the Effective Reproductive Number of SARS-CoV-2". In: *eLife* 11 (Aug. 2022). Ed. by Miles P Davenport, e71345. ISSN: 2050-084X. DOI: 10.7554/eLife.71345. (Visited on 02/05/2024).

[41] Bryan Wilder, Michael Mina, and Milind Tambe. "Tracking Disease Outbreaks from Sparse Data with Bayesian Inference". In: *Proceedings of the AAAI Conference on Artificial Intelligence* 35.6 (May 2021), pp. 4883–4891. ISSN: 2374-3468. DOI: 10.1609/aaai.v35i6.16621. (Visited on 10/27/2024).

[42] Andrea De Simone and Marco Piangerelli. "A Bayesian Approach for Monitoring Epidemics in Presence of Undetected Cases". In: *Chaos, Solitons & Fractals* 140 (Nov. 2020), p. 110167. ISSN: 0960-0779. DOI: 10.1016/j.chaos.2020.110167. (Visited on 10/27/2024).

[43] Samir Bhatt et al. "Semi-Mechanistic Bayesian Modelling of COVID-19 with Renewal Processes". In: *Journal of the Royal Statistical Society Series A: Statistics in Society* 186.4 (Oct. 2023), pp. 601–615. ISSN: 0964-1998. DOI: 10.1093/jrsssa/qnad030. (Visited on 10/27/2024).

[44] Katharine Sherratt et al. "Exploring Surveillance Data Biases When Estimating the Reproduction Number: With Insights into Subpopulation Transmission of COVID-19 in England". In: *Philosophical Transactions of the Royal Society B: Biological Sciences* 376.1829 (May 2021), p. 20200283. DOI: 10.1098/rstb.2020.0283. (Visited on 10/27/2024).

[45] R. N. Thompson et al. "Improved Inference of Time-Varying Reproduction Numbers during Infectious Disease Outbreaks". In: *Epidemics* 29 (Dec. 2019), p. 100356. ISSN: 1755-4365. DOI: 10.1016/j.epidem.2019.100356. (Visited on 09/09/2023).

[46] Luis Alvarez, Miguel Colom, and Jean-Michel Morel. *Removing Weekly Administrative Noise in the Daily Count of COVID-19 New Cases. Application to the Computation of Rt.* Nov. 2020. DOI: 10.1101/2020.11.16.20232405. (Visited on 10/27/2024).

[47] I. Ogi-Gittins et al. "A Simulation-Based Approach for Estimating the Time-Dependent Reproduction Number from Temporally Aggregated Disease Incidence Time Series Data". In: *Epidemics* 47 (2024), p. 100773. ISSN: 1755-4365. DOI: 10.1016/j.epidem.2024.100773. (Visited on 09/24/2024).

[48] Rebecca K. Nash et al. "Estimating the Epidemic Reproduction Number from Temporally Aggregated Incidence Data: A Statistical Modelling Approach and Software Tool". In: *PLOS Computational Biology* 19.8 (Aug. 2023). Ed. by Eric Hy Lau, e1011439. ISSN: 1553-7358. DOI: 10.1371/journal.pcbi.1011439. (Visited on 09/29/2023).

[49] Pierre Nouvellet et al. "A Simple Approach to Measure Transmissibility and Forecast Incidence". In: *Epidemics*. The RAPIDD Ebola Forecasting Challenge 22 (Mar. 2018), pp. 29–35. ISSN: 1755-4365. DOI: 10.1016/j.epidem.2017.02.012. (Visited on 10/27/2024).

[50] Nicholas Steyn and Kris V. Parag. *Robust Uncertainty Quantification in Popular Estimators of the Instantaneous Reproduction Number*. Oct. 2024. DOI: 10.1101/2024.10.22.24315918. (Visited on 10/25/2024).

[51] Nicolas Chopin and Omiros Papaspiliopoulos. *An Introduction to Sequential Monte Carlo*. Springer Series in Statistics. Cham: Springer International Publishing, 2020. ISBN: 978-3-030-47844-5 978-3-030-47845-2. DOI: 10.1007/978-3-030-47845-2. (Visited on 08/01/2024).

[52] Markus Hürzeler and Hans R. Künsch. "Approximating and Maximising the Likelihood for a General State-Space Model". In: *Sequential Monte Carlo Methods in Practice*. Ed. by Arnaud Doucet, Nando de Freitas, and Neil Gordon. Statistics for Engineering and Information Science. New York, NY: Springer, 2001, pp. 159–175. ISBN: 978-1-4757-3437-9. DOI: 10.1007/978-1-4757-3437-9_8. (Visited on 09/13/2023).

[53] Sarah F. McGough et al. "Nowcasting by Bayesian Smoothing: A Flexible, Generalizable Model for Real-Time Epidemic Tracking". In: *PLOS Computational Biology* 16.4 (Apr. 2020), e1007735. ISSN: 1553-7358. DOI: 10.1371/journal.pcbi.1007735. (Visited on 10/27/2024).